Overall Reaction Kinetics and Morphology of Austenite Decomposition between the Upper Nose and the M_s of a Hypoeutectoid Fe-C-Cr Alloy

H. GOLDENSTEIN and H.I. AARONSON

The overall transformation kinetics and microstructures of an Fe-0.13 pct C-2.99 pct Cr alloy were investigated above and below the bay temperature (T_b) with optical and electron metallography. Most of the kinetic and microstructural aspects of transformation are similar to their counterparts in Fe-C-Mo alloys. Transformation stasis (= incomplete transformation) was observed at all temperatures studied below T_b. However, nonmonotonic behavior of the percent transformation at stasis as a function of undercooling below T_b was found in the present alloy and attributed to a wider temperature interval below T_b in which the Widmanstätten structure is largely suppressed. Also, unlike Fe-C-Mo alloys, fibrous carbides form below as well as above T_b; in both Mo and Cr alloys, however, interphase boundary carbides appear in association with proeutectoid ferrite both above and below T_b. The solute drag-like effect, somewhat weaker in Fe-C-Cr than in Fe-C-Mo alloys, provides a qualitative explanation for most of the kinetic and microstructural observations made.

I. INTRODUCTION

TWO of the preceding papers in this journal report the results of detailed studies on the transformation kinetics and morphology of austenite decomposition products at and somewhat above the bay temperature[1] and at and somewhat below the bay temperature[2] in Fe-C-Mo alloys. The present investigation was undertaken to determine the overall reaction kinetics and the morphology of transformation at counterpart temperatures both above and below the bay in an Fe-C-Cr alloy. The primary purpose of this work was to ascertain which of the principal results secured on Fe-C-Mo appears to be generic to austenite decomposition in Fe-C-X alloys, where X is a strong carbide-forming substitutional alloying element and is present at a concentration high enough at the carbon concentration employed to produce a bay in the time-temperature-transformation (TTT) diagram and also the "incomplete transformation = transformation stasis"[3] phenomenon. The latter process has been defined as the cessation of ferrite or bainite formation prior to the appearance of the Lever Rule proportion of ferrite.[4]

Among the findings reported in Fe-C-Mo alloys, incomplete transformation is absent above the bay temperature, T_b (defined as the temperature in the intermediate transformation temperature region at which the isothermal reaction time required to initiate transformation passes through a maximum);[1,3] in this temperature region, isothermal reaction kinetics are invariably of the simple sigmoidal type.[1] Below the bay, however, up to four different patterns of overall reaction kinetics are observed.[2] At those temperatures where transformation stasis occurs, carbide precipitation at $\alpha:\gamma$ boundaries in association with the ferrite initially formed does not commence until the end of the stasis interval.[2] Ferrite morphology in Fe-C-Mo alloys exhibiting stasis displays marked differences[1,5] with respect to the usual pattern found in the proeutectoid ferrite and bainite regions of hypoeutectoid Fe-C, plain carbon steels, and many alloy steels. In the latter steels, grain boundary ferrite allotriomorphs predominate at high temperatures; with successive reductions in reaction temperature, Widmanstätten sideplates, and then intragranular plates, develop and become major features of the microstructure.[6–9] At still lower temperatures, individual ferrite plates are replaced by sheaves of parallel plates[7–10] (which become upper bainite in the presence of a nonlamellar dispersion of carbides) and then by parallel sideplates sympathetically nucleated edge-to-face at a roughly 55 deg angle[11] with respect to a "substrate" ferrite plate[12] (lower bainite when nonlamellar carbides are present). In the presence of sufficient proportions of Mo and C, however, a bay is introduced in the TTT curve for initiation of transformation. An "upper nose" and a "lower nose" thus appear in this curve. Below the upper nose, formation of ferrite plates is increasingly suppressed, until at T_b grain boundary and twin boundary allotriomorphs are the only ferrite morphologies present, particularly in higher Mo alloys.[1,5] Just below T_b, the allotriomorphs are supplemented by and then wholly replaced by a remarkably degenerate version of the Widmanstätten sideplate and intragranular plate morphologies.[5,13] This degeneracy slowly diminishes with decreasing reaction temperature[5] and also does so with increasing reaction time, though the latter effect appears to be largely a consequence of extensive impingement among adjacent ferrite plates.[13] Transmission electron microscopy (TEM) studies

H. GOLDENSTEIN, formerly Visiting Professor, Department of Metallurgical Engineering and Materials Science, Carnegie Mellon University, is Assistant Professor with the Department of Metallurgical Engineering, Escola Politecnica da Universidade de São Paulo, São Paulo, Brazil 05508. H.I. AARONSON, R.F. Mehl Professor, is with the Department of Metallurgical Engineering and Materials Science, Carnegie Mellon University, Pittsburgh, PA 15213.

This paper is based on a presentation made in the symposium "International Conference on Bainite" presented at the 1988 World Materials Congress in Chicago, IL, on September 26 and 27, 1988, under the auspices of the ASM INTERNATIONAL Phase Transformations Committee and the TMS Ferrous Metallurgy Committee.

have shown that carbide morphologies associated with ferrite in Fe-C-Mo alloys are of the interphase boundary and fibrous carbide types[14,15] above the bay.[16,17] Below the bay, fibrous carbides promptly disappear; interphase boundary carbides last until somewhat lower temperatures.[13] Large laths of Mo_2C appear at temperatures not too far below T_b; at lower temperatures, these are replaced by $(Fe, Mo)_3C$ laths.[13] This sequence of carbide morphologies is also not characteristic of either plain carbon steels or alloy steels whose TTT diagrams do not contain a bay at intermediate reaction temperatures.

In respect to austenite decomposition in reasonably pure Fe-C-Cr alloys, results previously reported which are relevant, either immediately or as fundamental background, to the present investigation may be summarized as follows. Davenport and Bain[18] were the first to demonstrate (in 1930) a bay in the TTT curves for an Fe-C-Cr alloy at intermediate reaction temperatures. Incomplete transformation in Fe-C-Cr alloys was reported by Wever and Jellinghaus[19] in 1932 and by Rose and Fischer[20] in 1939 using dilatometric and magnetic methods. Rose and Fischer[20] also found some deviations from sigmoidal behavior in overall reaction kinetics which they did not discuss in detail; these data will be considered in Section IV. Lyman and Troiano[21] interpreted dilatometric data on 3 pct Cr steels as showing that the maximum proportion of bainite formed, prior to the onset of transformation stasis, increases smoothly from zero to unity as the reaction temperature is reduced below T_b. Boswell *et al.*[5] have shown that sufficient proportions of C and Cr cause degeneration of the Widmanstätten morphologies at T_b in the same manner as they observed in Fe-C-Mo alloys, though the effect, per atomic percent X, is less severe in Fe-C-Cr alloys. Rose and Fischer[20] reported that decomposition of the austenite remaining after completion of stasis takes place through the pearlite reaction; however, it is no longer certain that this identification was securely accomplished. Klier and Lyman[22] and Lyman and Troiano,[21] using 3 pct Cr steels instead of the 0.24 to 2 pct Cr alloys employed by Rose and Fischer, stated that completion of transformation is accomplished by a dark-etching, nonpearlitic product. Reynolds *et al.*[2] used electron microscopy to show that the bainite reaction resumes after transformation stasis below T_b in Fe-C-Mo alloys. Similarly, "growth stasis" (though not transformation stasis), observed above T_b, is also terminated by the renewed formation of bainite indistinguishable from that appearing prior to growth stasis.[1] Mannerkoski,[14] Relander,[15] and Campbell and Honeycombe[23] observed both interphase boundary and fibrous carbides in high-Cr Fe-C-Cr alloys. While the absence of bulk partition of Cr between austenite and ferrite (now known to be mixtures of ferrite and carbides[17,23]) has been demonstrated by means of electron probe analysis in a 3 pct Cr alloy with nearly the same composition as that employed in the present investigation[24] and was later confirmed in two other 3 pct Cr alloys,[25] both $(Fe, Cr)_3C$ and Cr_7C_3 are formed in association with ferrite at high reaction temperatures.[26] Only $(Fe, Cr)_3C$ is observed at lower temperatures.[26] $(Fe, Cr)_7C_3$ is the equilibrium carbide in the alloy used in the present study.[27]

II. EXPERIMENTAL PROCEDURES

The alloy used in this investigation contained (in weight percent) 0.13 pct C, 2.99 pct Cr, 0.002 pct Mn, 0.001 pct Si, 0.001 pct P, and 0.006 pct S. The alloy was prepared at the Scientific Laboratory of Ford Motor Company, Dearborn, MI, by vacuum melting and casting followed by redundant hot working. After investigation of Cr distribution in austenite with electron probe microanalysis, the alloy was homogenized for 3 days at 1300 °C in a quartz capsule with a purified Ar atmosphere. Individual specimens $4 \times 10^{-4} \times 10^{-3} \times 10^{-3}$ m were austenitized for 15 minutes at 1300 °C in a graphite-deoxidized, argon-protected $BaCl_2$ bath,[28] yielding an austenite grain size varying from ASTM No. 2 to coarser than No. 1. Isothermal reaction was conducted in stirred, graphite-protected, graphite-deoxidized lead baths at temperatures from 700 °C to 525 °C and then quenched in iced brine. For optical metallographic examination, a broad face of these specimens was mechanically polished and then etched with Le Pera's reagent.[29,30] The volume fraction of austenite transformed was determined by means of point counting.[31,32] For examination with replication electron microscopy, specimens were given a final polish with a colloidal silica slurry, etched in nital, shadowed at an angle of approximately 15 deg with Pt, and then coated with a layer of carbon approximately 100 nm thick. These replicas were cut into 0.002 m square segments and then etched free of their specimens in 10 pct nital. Thin foil specimens were prepared by chemical thinning to approximately 100 μ and then jet polishing in 20 pct anhydrous sodium chromate in glacial acetic acid at room temperature and 40 to 60 V. Foils were observed in a JEOL 120CX microscope operated at 120 kV.

III. RESULTS

A. *Overall Reaction Kinetics*

Figure 1 presents the TTT diagram for the alloy investigated within the temperature range studied. The

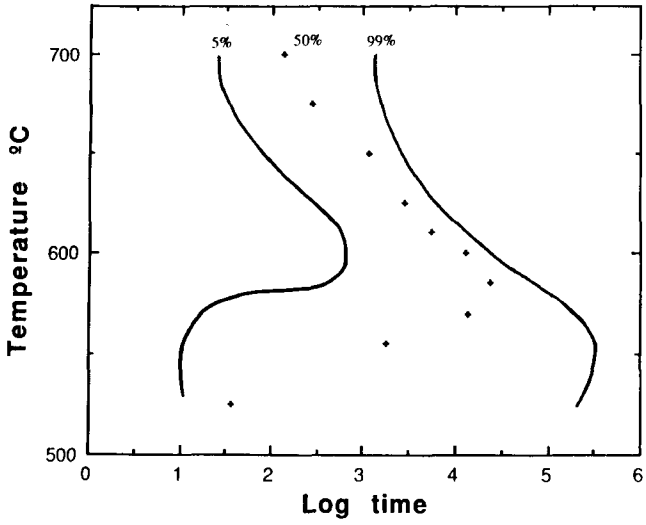

Fig. 1—TTT diagram at temperatures below the upper nose (approximately 700 °C) and the M_s (approximately 500 °C) of an Fe-0.13 pct C-2.99 pct Cr alloy.

dramatic increase in the time differences between the 50 and 99 pct transformation curves at temperatures below that of the bay (T_b is approximately 600 °C), familiar from previous investigations,[20,21] provides an initial indication (though not proof) of the presence of incomplete transformation. Figures 2(a) through (j) are isothermal reaction curves at each of the reaction temperatures utilized. In discussing these curves, the classification scheme described in Figure 2(k)[2,33] will be employed. Note that only the middle stage of Type IV kinetic behavior corresponds to transformation stasis. Figures 2(a) through (f), representing reaction temperatures from 700 °C down

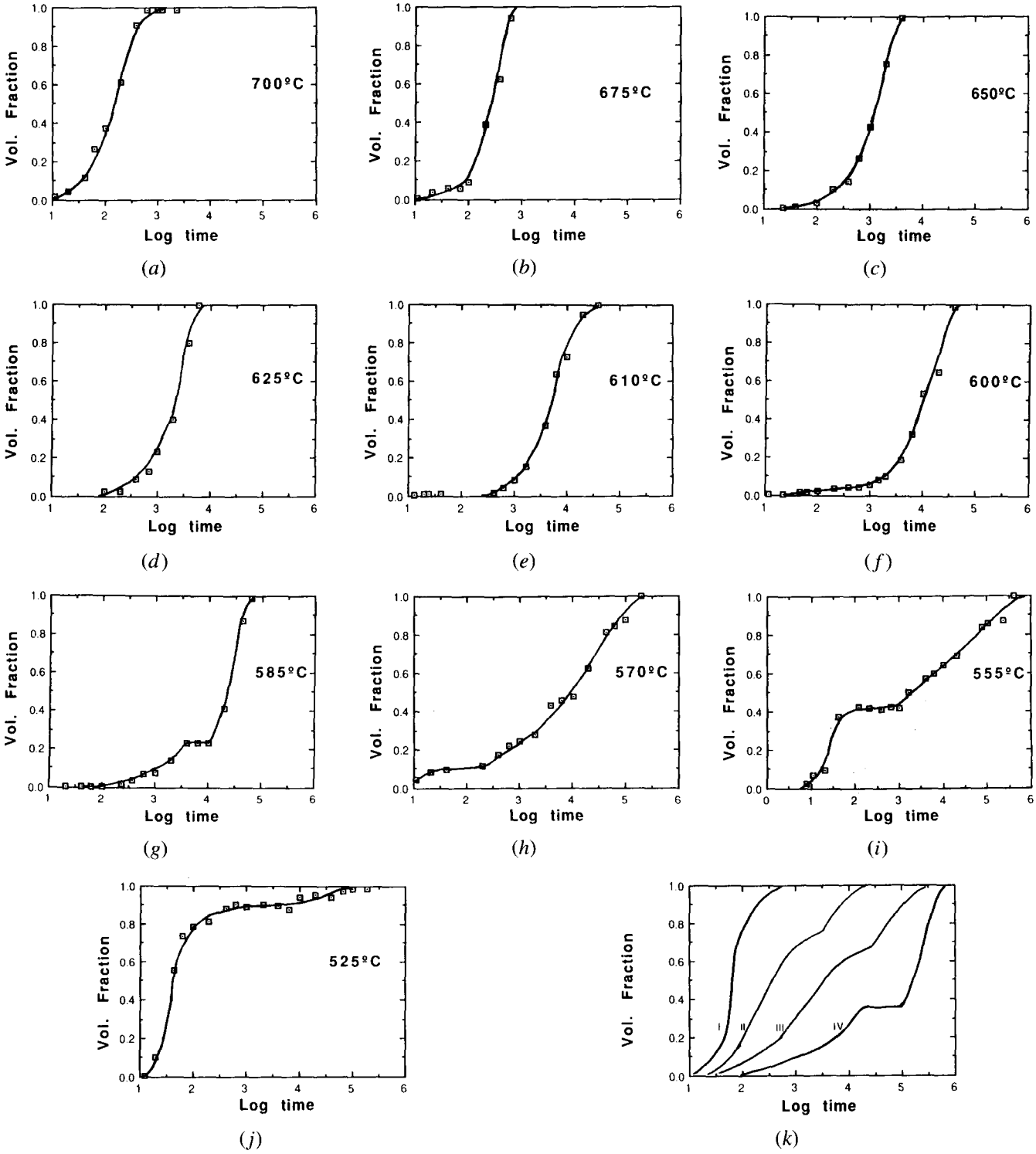

Fig. 2—Percentage of austenite isothermally transformed as a function of the isothermal reaction time at (*a*) 700 °C, (*b*) 675 °C, (*c*) 650 °C, (*d*) 625 °C, (*e*) 610 °C, (*f*) 600 °C, (*g*) 585 °C, (*h*) 570 °C, (*i*) 555 °C, and (*j*) 525 °C. (*k*) The types of isothermal reaction curves found below the bay temperature.[2,33]

to 600 °C are all properly described by the Type I, *i.e.*, sigmoidal or "Johnson-Mehl," [34] form of overall transformation kinetics. Figures 2(g) through (j), on the other hand, presenting the overall kinetics from 585 °C through 525 °C, all display Type IV behavior. Except in one particular case, these results are those classically accepted for bainite described by the overall reaction kinetics definition, *e.g.*, Reference 35. This exception is that the percent transformation at which stasis occurs does not increase smoothly with undercooling below T_b. Instead, this quantity is 25 pct at 585 °C, 12 pct at 570 °C, 42 pct at 555 °C, and 90 pct at 525 °C. The percent transformation required to develop stasis at 585 °C is thus anomalously high. An explanation for this anomaly will become apparent when the microstructures associated with these transformation temperatures are examined.

B. *Optical Microstructures*

Figure 3 illustrates a typical Widmanstätten ferrite microstructure developed at 700 °C, the upper nose in the TTT curve for initiation of transformation. These plates exhibit the Type A degeneracy observed among sideplates in a plain carbon steel (0.29 pct C, 0.76 pct Mn, 0.25 pct Si), particularly as illustrated in Figures 47(a) and (f) and 48(a) of Reference 36. This is one of three crystallographically based forms of ferrite sideplate degeneracy identified in this steel. These degeneracies also occur in alloy steels, and it is important to distinguish them from the below-T_b degeneracies characteristic of Fe-C-Mo and Fe-C-Cr alloys when sufficient proportions of C and X are present. With decreasing reaction temperature, the Widmanstätten structure diminishes in importance. As illustrated in Figure 4, however, it remains an important feature of the microstructure. The Widmanstätten morphology now undergoes a somewhat subtle change in its detailed shape. As shown in Figure 4, the degeneracy changes from the pronouncedly crystallographic style of Figure 3 to the more irregular, quasi-random mode of sub-bay degeneracy. Comparison with Figures 11 and 12 of the paper by Boswell *et al.*[5] on Fe-C-Mo alloys demonstrates that Cr induces the same type of degeneracy among ferrite plates formed at the bay (Figure 4) and just below the bay (Figure 5), as does Mo. Figure 5, taken of a specimen reacted at 585 °C during the stasis interval, shows the same type of degeneracy as Figure 4 reacted at 600 °C (T_b) and also demonstrates that Cr has now further suppressed the Widmanstätten morphology. Figure 6 is a higher magnification view of sideplate degeneracy at 585 °C. Although the irregularities displayed would almost certainly have a more crystallographic appearance when viewed at the much higher resolutions permitted by TEM, the seemingly random nature of the degeneracy and the blurred outline of individual plates are again apparent in this higher magnification illustration.

Figure 7 demonstrates that while ferrite plates are still degenerate at 570 °C, the crystallographic appearance characteristic of this morphology has now returned and parallel planarities of $\alpha:\gamma$ boundaries again strongly influence the appearance of the microstructure. Again,

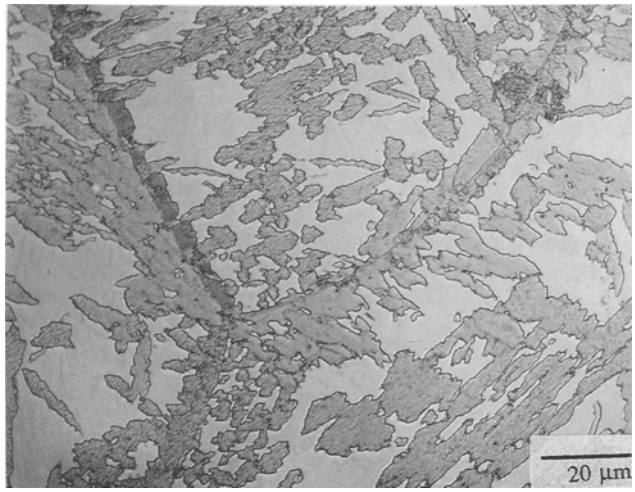

Fig. 4—Degenerate Widmanstätten structure of a more irregular type developed at the bay temperature. Reacted 4020 s at 600 °C.

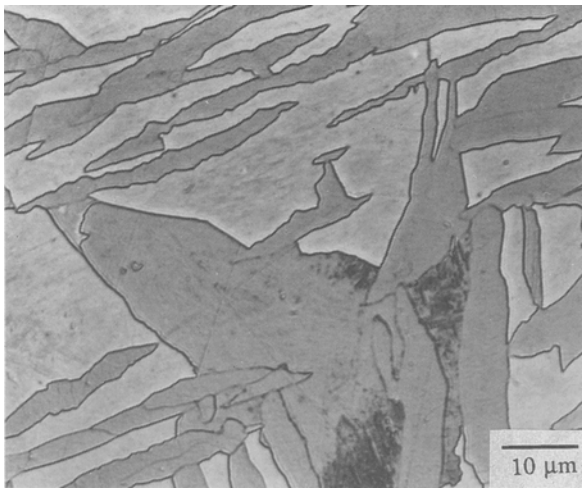

Fig. 3—Crystallographically degenerate ferrite plates with unresolved eutectoid structure beginning to form in the austenite trapped between them. Reacted 200 s at 700 °C.

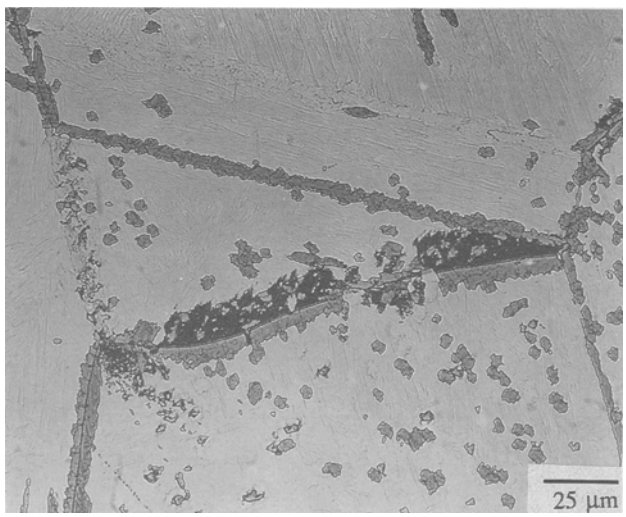

Fig. 5—Only a small amount of Widmanstätten structure is present after reaction 15 °C below the bay temperature in a microstructure of which grain boundary and twin boundary allotriomorphs are now a major component. Reacted 6300 s at 585 °C.

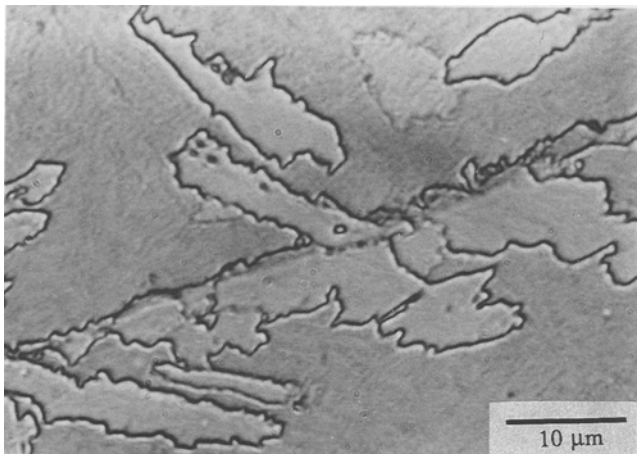

Fig. 6—Higher magnification optical micrograph of a sub-bay degenerate ferrite. Note gray-etching, unresolved eutectoid structure above the austenite grain boundary passing laterally across the micrograph. Reacted 2820 s at 585 °C.

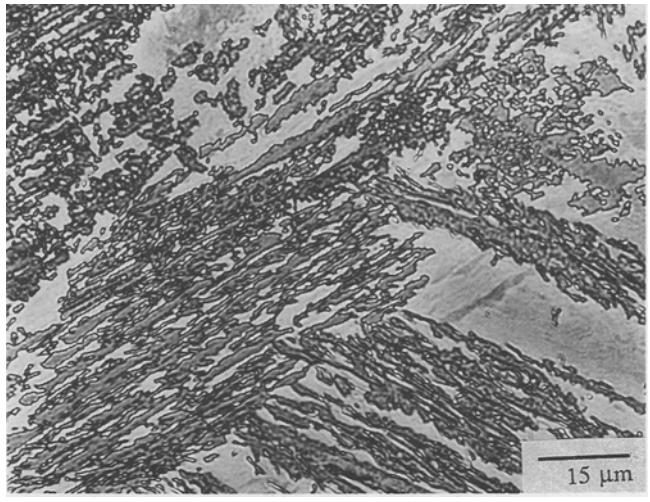

Fig. 8—Further reduction of Widmanstätten structure degeneracy at a still lower temperature. Reacted 400 s at 555 °C.

Boswell *et al.*[5] made equivalent observations on Fe-C-Mo alloys (compare their Figures 12 (630 °C) and 13 (600 °C), taken of an Fe-0.11 pct C-1.95 pct Mo alloy whose T_b = 650 °C, with our Figures 6 and 7). That further undercooling of the present alloy causes additional diminution in "sub-bay" degeneracy, now at a slower rate, is shown by comparison of Figure 8, taken after reaction in the stasis region at 555 °C, with Figure 7.

Although the eutectoid structures developed within the temperature range studied in this alloy formed on too fine a scale to permit resolution of individual carbides with optical microscopy, a brief overview of the external morphology, distribution, and proportion of these structures is, nonetheless, an important part of the present "story." While all of the ferrite structures so far described sooner or later contained carbides, their external morphology was largely determined by the growth kinetics and mechanisms of the ferrite phase. At later reaction times, however, eutectoid structures appeared in which, as recently described,[33,37] the external morphology was jointly determined by crystals of the ferrite and carbide phases. Pearlite was observed at 700 °C in the present alloy but not at 675 °C or at any lower temperature. Figure 9 shows the external shape of the eutectoid structures developed at reaction temperatures from 675 °C to 570 °C. Figure 9(a) displays clearly the nodular external shape of these structures at 675 °C. Even when filling in the austenite left untransformed between complexes of ferrite crystals (which have been closely enveloped themselves by unresolved eutectoid structures), as in Figure 9(b) (650 °C), the nodular morphology of the eutectoid structure which transformed the remaining austenite is clearly evident. Figure 9(c) shows that at 610 °C, just above the bay temperature, most of the austenite matrix is transformed to bainite nodules rather than to ferrite-dominated structures. Figures 9(d) through (f) illustrate the role of the nodular eutectoid structure in decomposing progressively diminishing volumes of austenite not previously transformed to ferrite-dominated structures as the reaction temperature is successively decreased to 600 °C, 585 °C, and 570 °C. The eutectoid microstructures at late stages of transformation at 555 °C and 525 °C are not easily distinguished from that at 570 °C and, hence, are not illustrated here.

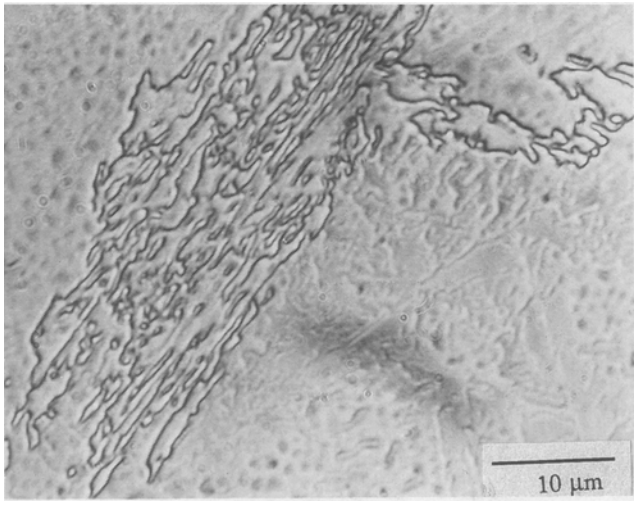

Fig. 7—Partial recovery of linear-sided Widmanstätten structure at a lower reaction temperature. Reacted 260 s at 570 °C.

C. *Electron Microstructures*

Both replication and transmission electron microscopy were used to resolve and elucidate the nature of the various ferrite + carbide structures developed. Figure 10 is a good example of the carbide structure within nodular bainite. This morphology is basically the same as that of nodular bainite, as observed in an Fe-0.24 pct C-0.93 pct Mo alloy (Figure 1(b) of Reference 38), a hypoeutectoid Ti-Cr alloy (Figures 9(a) and (b) of Reference 39), and a hypereutectoid Ti-Cr alloy (Figures 5(a) and (b) of Reference 40).

Interphase boundary carbides and fibrous carbides associated with proeutectoid ferrite crystals, usually though not always in the allotriomorphic morphology, are now a well-accepted feature of the electron microstructure of

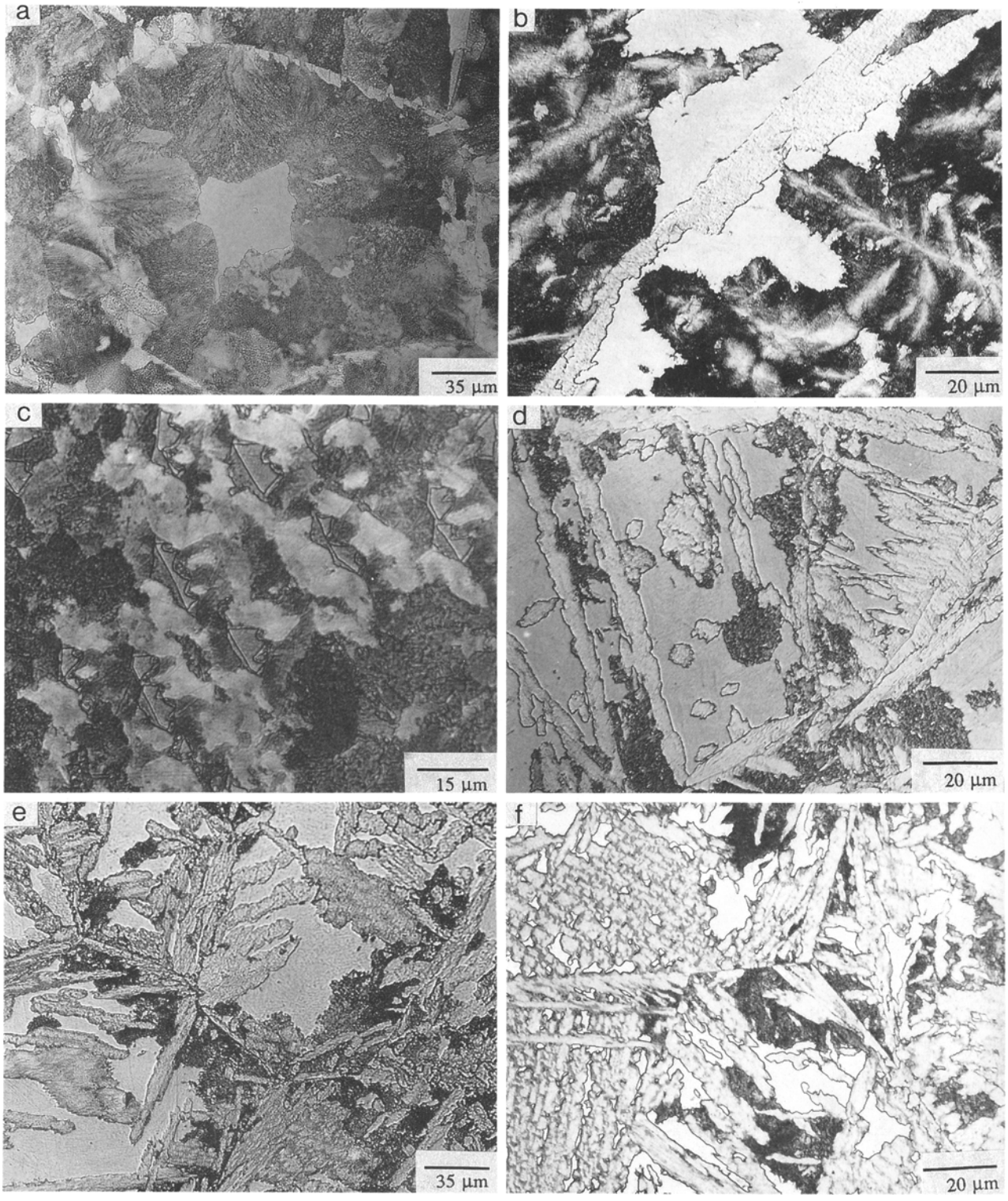

Fig. 9—Optical micrographs of eutectoid structures developed at successively decreasing reaction temperatures: (*a*) 675 °C/630 s; (*b*) 650 °C/1980 s; (*c*) 610 °C/20,040 s; (*d*) 600 °C/10,080 s; (*e*) 585 °C/42,000 s; and (*f*) 570 °C/20,220 s.

hypoeutectoid (and approximately eutectoid) steels containing appreciable proportions of one or more strong carbide-forming alloying elements, such as Cr or Mo.[16,17,26] Figure 11 is a TEM micrograph of interphase boundary carbides, here, in a partially curvilinear mode,[23,41–43] as a consequence of greater complexities in the modus operandi of the ledge mechanisms.[44] Figure 12 is a replication micrograph of an uncommonly regular fibrous structure. As a contribution toward understanding the origin of this structure, Figure 13 shows the initial stages in the evolution of sideneedles from approximately equiaxed carbide crystals nucleated at an $\alpha:\gamma$

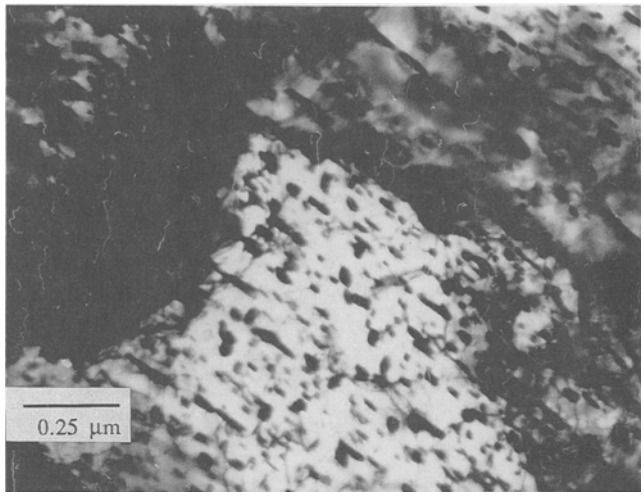

Fig. 10—TEM micrograph showing internal structure of nodular bainite. Reacted 20,040 s at 570 °C.

boundary. The spacing between adjacent sideneedles in Figure 13 is nearly the same as that between adjacent fibers in Figure 12.

A less familiar carbide morphology is shown in Figure 14 in the form of ribbons. Branching of these ribbons, presumably by sympathetic nucleation, is seen to be a mechanism through which their numbers can be multiplied. An equivalent carbide microstructure has been reported by Bee and Edmonds[45] in Fe-0.21 pct C-3.13 pct Mo and Fe-0.5 pct C-10.4 pct Cr alloys. They have also been observed, more frequently than in the present alloy, in an Fe-0.22 pct C-10.6 pct Cr steel.[26]

One further, somewhat more subtle, ferrite + carbide microstructure was observed. This consists of small ferrite sideplates, obviously developed at a late stage of transformation, within which carbides are embedded. A microstructure of this type is shown in Figure 15, with arrows pointing out some examples of carbides. Hultgren[46] observed this structure in an Fe-0.54 pct C-0.82 pct Mo alloy reacted at its bay temperature, as did

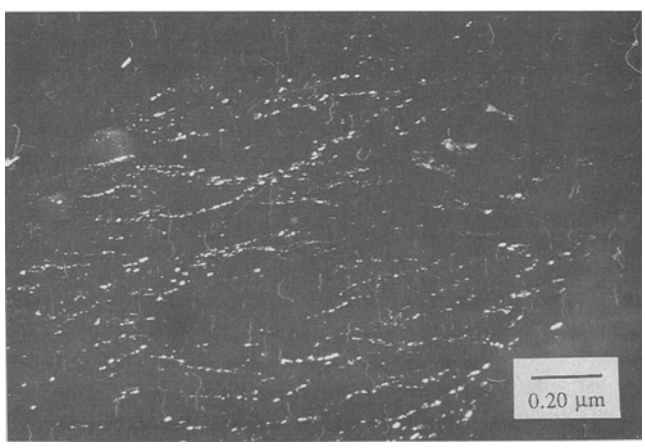

Fig. 11—Dark-field TEM micrograph of interphase boundary carbide structure imaged with a carbide reflection. Reacted 10,020 s at 585 °C.

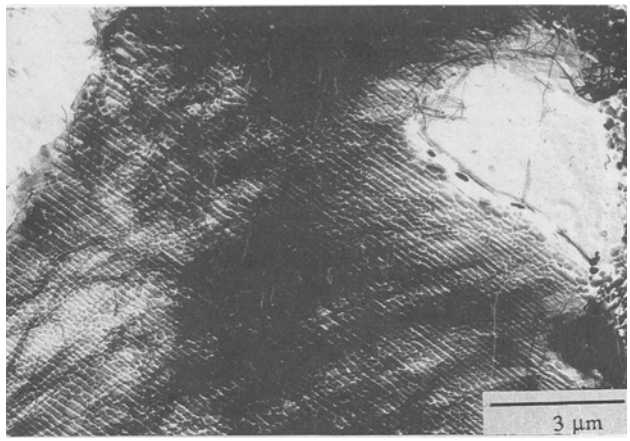

Fig. 12—Replication micrograph of an array of fibrous carbides. Reacted 15,900 s at 675 °C.

Habraken and Economopoulos[47] in a complex commercial steel. Hultgren described the sideplates as "shoots." Figure 16 shows shoots developing at some large ferrite crystals nucleated at austenite grain boundaries. The shoots have formed at the $\alpha:\gamma$ boundaries occupying approximately the former locations of the grain boundaries. While transformation stasis was still in progress at the time isothermal reaction of this specimen was terminated, the observations of this investigation indicate that when carbides have formed at an appreciable proportion of the $\alpha:\gamma$ boundaries present, transformation resumes with detectable kinetics. These carbides can develop as a component of shoot structures but do so more frequently as part of either fibrous carbide or interphase boundary carbide arrays. The dark-etching, unresolved fringe in Figure 6, similarly replacing an austenite grain boundary, is the optical micrographic equivalent of either Figure 16 or an equivalent structure of fibrous or interphase boundary carbides.

Figures 17 and 18 are montages of bright- and dark-field TEM micrographs, respectively, taken of a eutectoid structure developed from a possibly allotriomorphic array of ferrite crystals. There are some indications that the carbides are of the interphase boundary type, though the tilt angle of the thin foil with respect to the electron beam was unfortunately not optimized for visualizing this type of microstructure. By utilizing both of these montages, one can establish fairly well that the ferritic component of the interphase boundary carbide structure did not form by the continued growth of the proeutectoid ferrite substrate crystals. Instead, well-defined boundaries separate the "eutectoid ferrite" from the "proeutectoid ferrite." Upon closer examination, these boundaries, in some instances, can be seen to contain closely spaced dislocations, indicating that they are probably of the small-angle type. From the observations of Reynolds *et al.*[38] on Fe-C-Mo alloys and of Menon and Aaronson[48] on a Ti-Cr alloy, this indicates that the eutectoid ferrite was almost certainly formed by sympathetic nucleation[10] at austenite:proeutectoid ferrite boundaries. As will be noted in Section IV, this observation provides further evidence for an important aspect of the mechanism of the bainite reaction.

Fig. 13—Replication micrograph of fibers developing from carbides nucleated at an $\alpha:\gamma$ boundary. Reacted 200 s at 700 °C.

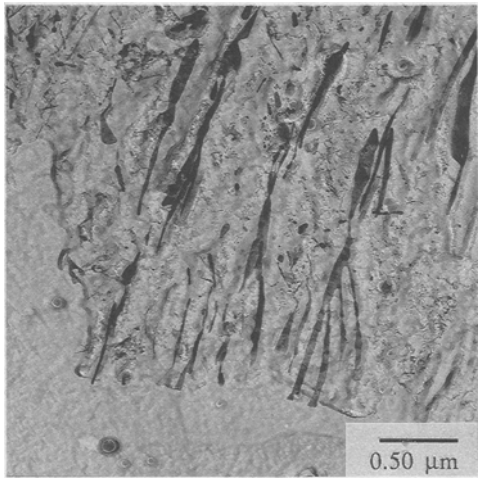

Fig. 14—Replication micrograph of ribbon-type carbides with branching. Carbides are in a ferrite matrix but are in contact with martensite matrix (lower left-hand corner of micrograph). Reacted 20,040 s at 585 °C.

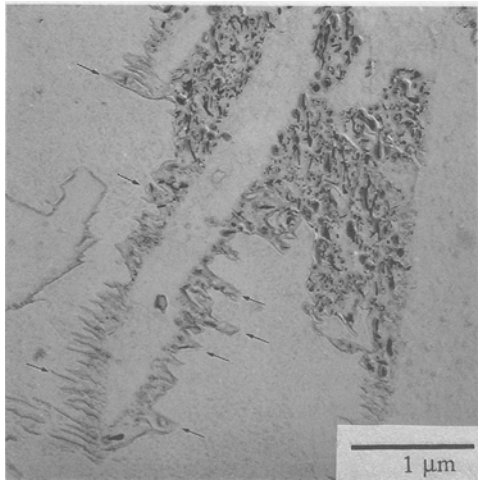

Fig. 15—Shoots of ferrite emerging from the sides of ferrite plates with carbides embedded among them along former $\alpha:\gamma$ boundaries. Reacted 10,200 s at 555 °C.

IV. DISCUSSION

A. *Solute Drag-Like Effect Explanation for Effects of Cr on Ferrite and Carbide Formation*

As in Fe-C-Mo alloys,[1,2,5,13,49] the solute drag-like effect (SDLE) appears to be the best explanation presently available for the differences in overall transformation kinetics, ferrite morphology, and carbide morphology and distribution between those reported here and previously in Fe-C-Cr alloys and those observed in Fe-C alloys, plain carbon steels, and alloy steels which exhibit neither a bay in their TTT diagram nor transformation stasis. In its present form, as described in another paper in this issue,[2] the SDLE is based upon the gradual sweeping up of a nonequilibrium concentration of an alloying element which markedly decreases the activity of carbon in austenite at the mobile areas of advancing $\alpha:\gamma$ boundaries. (These areas necessarily have a disordered structure;[50] on an atomic scale, their effective area now appears to be usually no more than that of kinks on the risers of growth ledges on $\alpha:\gamma$ boundaries.[51]) The X concentration thus adsorbed diminishes the carbon activity gradient in austenite, driving the growth of ferrite

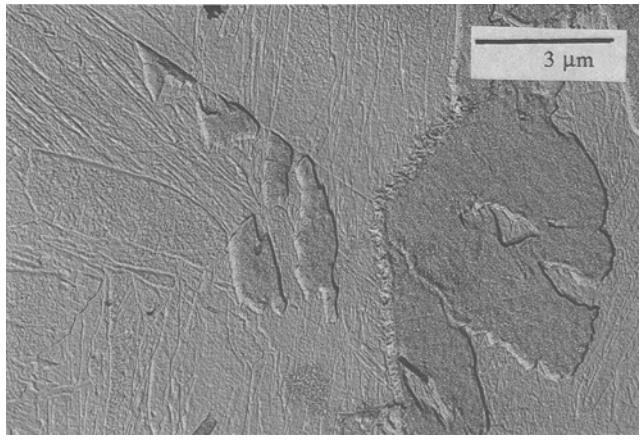

Fig. 16—Fringe of "shoot" structure round ferrite crystals nucleated at austenite grain boundaries. Reacted 100 s at 570 °C.

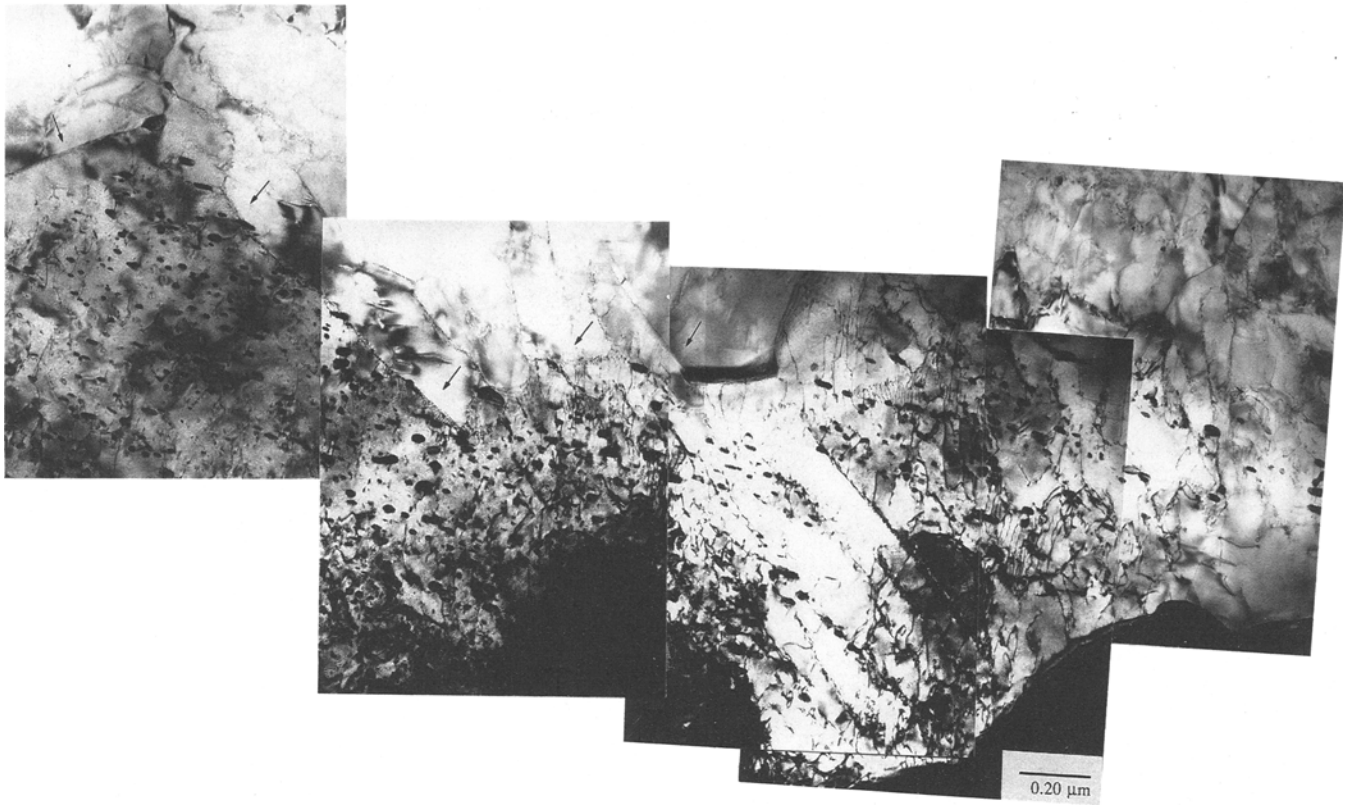

Fig. 17—Montage of bright-field TEM micrographs showing probable small-angle ferrite:ferrite boundaries between proeutectoid ferrite crystals and interphase boundary carbide structure. Arrows indicate some locations of these boundaries. Reacted 20,040 s at 570 °C.

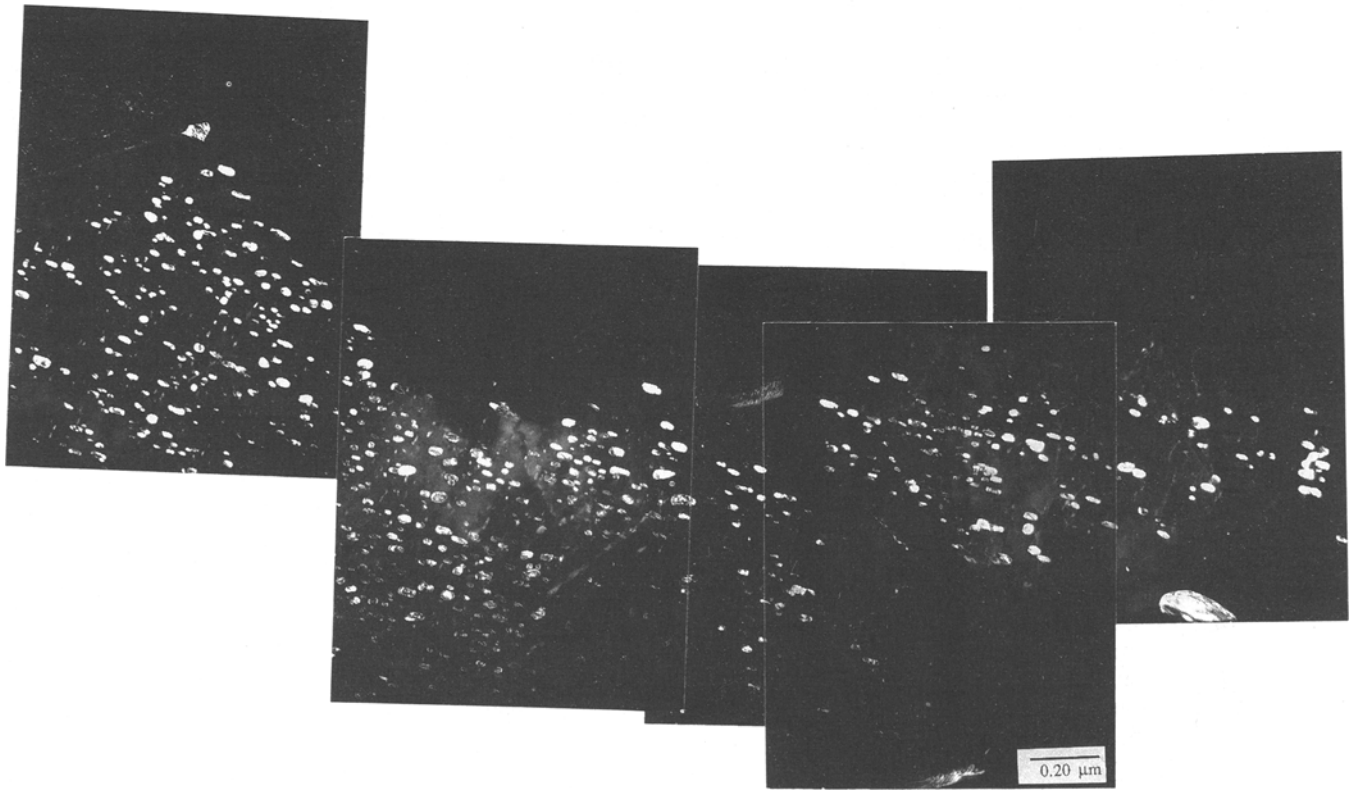

Fig. 18—Same as Fig. 17 but in a dark field.

under paraequilibrium[52] conditions.[53] When this gradient is reduced to zero, growth stasis occurs.[53] If all ferrite crystals in a specimen are simultaneously in growth stasis, despite the spectrum of times over which they have nucleated, then transformation stasis occurs.[1] When the SDLE is sufficiently strong, another factor enters which eventually expedites the development of both growth and transformation stasis, even though it works initially in the opposite sense. The reduction in the lateral migration rate of growth ledges (and likely also in the rate of ledge generation) provides enhanced opportunities for the sympathetic nucleation of new ferrite crystals at the terraces of growth ledges.[2] The newly formed ferrite crystals can grow rapidly, albeit at a continuously diminishing rate,[1,2] until they have accumulated a sufficient concentration of X at the mobile areas of their $\alpha:\gamma$ boundaries to enter growth stasis, whereupon the process repeats.[1,2] However, when the interiors of austenite grains contain a sufficient number of sympathetically nucleated ferrite crystals for a time long enough so that the minimum carbon concentration in the remaining austenite rises appreciably above that of the bulk carbon concentration in the alloy, the driving force for sympathetic nucleation is soon diminished sufficiently to prevent further nucleation. In this manner, the isothermal reaction time and perhaps even the proportion of ferrite required to induce transformation stasis should be significantly reduced, inasmuch as the average diffusion distance required to produce overlap of the carbon diffusion fields of nearby ferrite crystals will be materially diminished when allotriomorphs growing uniformly from the grain boundaries toward the interiors of austenite grains are replaced by the "skeletal" degenerate Widmanstätten morphology[5] produced by repeated sympathetic nucleation and by both the more nearly isotropic growth resulting from additional X adsorption at the more disordered areas of $\alpha:\gamma$ boundaries[5] and by the more extensive formation of high superledges at $\alpha:\gamma$ boundaries.[2] This increase in the carbon concentration throughout the remaining untransformed austenite also further diminishes the carbon activity gradient driving growth. Hence, the occurrence of both growth and transformation stasis takes place sooner than in the situation where ferrite growth is largely confined to the thickening of grain boundary allotriomorphs.

The anomalously high percent transformation at which transformation stasis occurs at 585 °C—25 pct instead of roughly 6 pct (since T_b = 600 °C and stasis occurs at 12 pct transformation during reaction at 570 °C)—provides a useful test of the sympathetic nucleation/degenerate ferrite component of the SDLE explanation of growth and transformation stasis. Figure 5 demonstrates that during stasis of 585 °C, only a small proportion of degenerate Widmanstätten structure is present. Hence, stasis must be accomplished mainly by reduction of the carbon activity in austenite in contact with $\alpha:\gamma$ boundaries to that of the austenite in the bulk alloy. However, Figure 19 shows (here somewhat after completion of stasis) that the degenerate Widmanstätten structure develops rapidly throughout the interiors of the austenite grains at 570 °C, thereby permitting (as just described) increases in the activity of carbon in the regions of austenite furthest away from the advancing $\alpha:\gamma$ boundaries to contribute to reduction in the driving force for the growth of ferrite. The increased driving force available for sympathetic nucleation as the reaction temperature was reduced from 585 °C to 570 °C is probably primarily responsible for the more rapid and extensive formation of degenerate structure at the lower temperature, since sympathetic nucleation has now been recognized[2] as a major contributor to the development of this special variant of the Widmanstätten plate morphology.

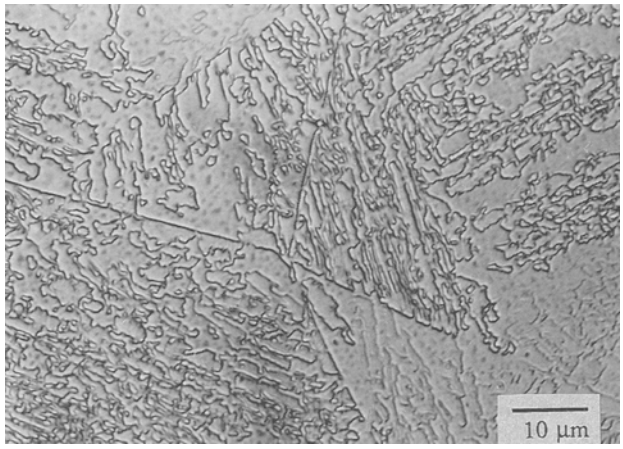

Fig. 19—Return of the Widmanstätten structure in large quantities upon further undercooling below the bay temperature. Reacted 260 s at 570 °C.

Diminution of the frequency with which Widmanstätten morphologies appear between the upper nose in the TTT diagram and T_b, degeneration of the Widmanstätten morphologies below T_b, and development of incomplete transformation below the bay (with the exception discussed in the preceding paragraph) are all qualitatively the same as in Fe-C-Mo alloys.[1,2,5,13] As Boswell *et al.*[5] noted and the present study confirms in more detail, Cr is less effective, per atomic percent X, than Mo in producing these effects. Since the influence of Cr upon the activity of carbon in austenite is nearly the same as that of Mo,[54] one may suggest instead that the smaller atomic size difference between Cr and Fe than between Mo and Fe results in a lesser tendency for Cr to be adsorbed at a given type of $\alpha:\gamma$ boundary.[55] Continuation of fibrous carbide formation to temperatures appreciably below that of T_b in Cr but not in Mo alloys likely results from the lesser degeneracy of the ferrite formed in Fe-C-Cr alloys. The severe nature of this degeneracy in Fe-C-Mo alloys, it has been suggested,[13] inhibits uniform development of parallel fibers, since this requires that the $\alpha:\gamma$ boundaries from which they develop retain an approximately constant orientation over an appreciable area if a "colony" of fibrous carbides is to develop, as illustrated in Figure 13.

The "shoot"[46] microstructure (Figure 15) is also explicable on the basis of the SDLE. Carbide precipitation at $\alpha:\gamma$ boundaries drains Cr from them through diffusion along these boundaries. Local diminution of the SDLE follows. The anisotropy of $\alpha:\gamma$ boundary mobility which obtains at these temperatures in the absence of the SDLE (*i.e.*, in Fe-C alloys and plain carbon steels[6]) can thus develop locally, leading to the formation of sideplates.

The observation by Hultgren[46] of this microstructure in an Fe-C-Mo alloy, previously noted, is indicative of the generality of this morphological development and provides some further support for the SDLE-based explanation offered.

B. *Overall Reaction Kinetics Behaviors*

Lyman and Troiano[21] determined the upper and lower limiting temperatures of incomplete transformation as a function of carbon concentration in 3 pct Cr steels. On the extrapolation that T_b in the present alloy is that at which stasis began at 0 pct transformation, this temperature is in good agreement with that interpolated from their plot of T_b *vs* percent C. However, at carbon concentrations ranging from 0.08 to 1.02 pct, they found that the total dilatometric expansion at the time transformation stasis began increased smoothly as the reaction temperature was decreased below T_b. The anomaly found during the present study in the percent transformation at stasis as a function of reaction temperature is not consistent with their results. In view of the small intervals of reaction temperature which Lyman and Troiano were able to employ and the wide range of total expansions they found at each temperature, it is surprising that this anomaly was not detected with dilatometry.

Lyman and Troiano[21] did not present any plots of dilatometric expansion *vs* isothermal reaction time. Rose and Fischer,[20] however, showed a series of isothermal transformation curves, determined by a magnetic technique, in both the pearlite and bainite ranges of a 0.64 pct C, 1.32 pct Cr steel (also containing 0.17 pct Mn and 0.26 pct Si). In this alloy, the pearlite and bainite reactions did overlap appreciably. Further, isothermal reaction times utilized did not extend beyond 400 seconds. None of the isothermal reaction curves presented exhibited Type IV behavior (Figure 2(k)) demonstrating transformation stasis. Only Type I and II behaviors were shown. It is possible that Type IV kinetics, including transformation stasis, would have developed at higher temperatures in the absence of the pearlite reaction. On the findings of Reynolds *et al.*[2] on Fe-C-Mo alloys, however, it is also possible that transformation stasis may not occur at any temperature in this alloy.

The absence of Type II and III behaviors in the present alloy may have resulted from the circumstance that the combination of C and Cr concentrations was sufficient to place this alloy far enough into the composition region in which stasis occurs so that Type IV behavior could prevail at all temperatures studied. In Fe-C-Mo alloys, it was found that Type III behavior, in particular, developed in alloys located closer to the C-Mo concentration region in which transformation stasis did not occur at any temperature below T_b.

C. *Development of Bainite Nodules*

The proposal has been recently made that the approximately equiaxed nodule is the fundamental morphology of microstructurally defined bainite.[37] The much more familiar plate morphologies, *e.g.*, upper and lower bainite in steel as well as allotriomorphic and inverse bainite, were suggested to be derivative morphologies reflecting primarily the morphology of the substrate proeutectoid phase crystal (or grouping of crystals) at which formation of a particular bainitic aggregate morphology was initiated.[33,37] Conditions which must be fulfilled for the development of nodular bainite were deduced[37] and applied to experimental observations in both Ti-Cr alloys[37,40,56] and steels.[37,38,57] These conditions, here stated in the terminology of austenite decomposition, include the following: (1) substantial contiguous volumes of untransformed austenite; (2) much higher nucleation rates of carbide at eutectoid ferrite:austenite than at proeutectoid ferrite:austenite boundaries; and (3) much more rapid formation of growth ledges at the former than at the latter boundaries. Conditions (2) and (3) lead to higher and more nearly isotropic growth kinetics of eutectoid than of proeutectoid ferrite, especially at late stages in the proeutectoid ferrite reaction. The two product phases of eutectoid decomposition, ferrite and carbide, now become more nearly equal partners in governing the kinetics and morphology of growth. Until the closing stages of austenite decomposition, when the nodular morphology must assume the shape of the volumes of austenite remaining untransformed, the external morphology of nodular bainite is approximately equiaxed, *i.e.*, about spherical in the interiors of austenite grains and roughly hemispherical at grain boundaries.[40,57] Particularly when the internal structure of nodular bainite is not fully resolved or when the carbides in bainite nodules are elongated in the direction of growth, there is a pronounced tendency to mistake nodular bainite for pearlite.[57,58]

By discouraging the development of both sideplates and intragranular plates, the SDLE provides the large contiguous volumes of unoccupied austenite constituting condition (1) for nodular bainite formation. This is particularly well illustrated in Figure 9(a). Even at lower reaction temperatures, when appreciable numbers of degenerate Widmanstätten structures have developed within austenite grains, the other components of Figure 9 demonstrate that relatively "bulky" regions of austenite remain untransformed and are thus available for the development of nodular bainite.

D. *Continued Growth (Hultgren) vs Sympathetic Nucleation Mechanisms of Eutectoid Ferrite Formation*

The last issue to be considered is that of the Hultgren[8] mechanism for the formation of the ferritic component of (upper) bainite and, more generally, for the development of the majority phase of a bainitic microstructure when this phase is the same as the proeutectoid phase formed before eutectoid decomposition began. Hultgren made the logical proposal that carbide precipitation at $\alpha:\gamma$ boundaries should expedite continued growth of the ferrite around the carbides because of the local increase in the driving force for ferrite growth. However, by taking advantage of the slower transformation rates of the (hcp) proeutectoid α reaction in a hypoeutectoid Ti-Co alloy and of retention of the untransformed (bcc) β matrix phase during quenching to room temperature following isothermal transformation, it was shown by means of TEM that "eutectoid α" formed beyond a line of Ti_2Co crystals precipitated at proeutectoid $\alpha:\beta$ boundaries was separated from its proeutectoid α substrate by small-angle

$\alpha:\alpha$ boundaries.[39] Such boundaries have been shown to separate sympathetically nucleated proeutectoid α crystals from the proeutectoid α crystals against which they were nucleated.[48] These boundaries are also present between the irregular ferrite crystals which, aligned in ragged rows through sympathetic nucleation, constitute the degenerate Widmanstätten structure characteristic of incomplete transformation in Fe-C-Mo,[2] Fe-C-Mn,[59] and Fe-C-Cr[21] (the present investigation) alloys. Figures 17 and 18 demonstrate the same phenomenon on a larger scale. Instead of just one row or sheet of carbides or Ti_2Co crystals, many such rows, each separated by eutectoid (*i.e.*, bainitic) ferrite, are present within the bainite nodule encompassed by the montages of Figures 17 and 18. Note that additional small-angle boundaries can be discerned within this structure. This suggests that repeated sympathetic nucleation of eutectoid ferrite occurred during the formation of this structure.

One is tempted to propose, by analogy to grain growth phenomena in pure metals and solid solutions, that carbide precipitation at $\alpha:\gamma$ boundaries has temporarily pinned these boundaries, thus requiring sympathetic nucleation in order to reinitiate ferrite formation. However, experimental evidence and theory are accumulating to indicate that carbides nucleate only rarely on moving $\alpha:\gamma$ boundaries. Instead, carbide nucleation must take place at the immobile terraces of ledges or at other interfaces immobilized by the SDLE.[2,60–62] A more satisfactory alternative mechanism is that carbide precipitation takes place when either the growth ledge density on $\alpha:\gamma$ boundaries is low or the driving force for growth has been seriously depleted. When adjacent parallel sideplates have thickened nearly into contact with each other, to the point where almost the Lever Rule proportion of ferrite has locally precipitated, the driving force for growth will approach zero. Under this circumstance, the results of Aikin and Plichta[63] on the coarsening kinetics of Θ' Al-Cu plates suggest the nucleation rate of new growth ledges is also sharply reduced. Even in the absence of a reduced driving force, however, it has often been found that at later stages of growth, the kinetics of growth ledge formation, by whatever mechanism, tend to be diminished, to a considerable extent, in several alloy systems.[51,65] This circumstance is favorable to the occurrence of sympathetic nucleation. Hence, it would now appear that the following sequence may obtain during the initial precipitation of carbides and subsequent stages of the bainite reaction (as defined microstructurally[33,53,64] rather than on the basis of overall reaction kinetics):

(1) growth ledge density at and near a particular boundary orientation is markedly diminished;
(2) carbide nucleation occurs at terraces between widely separated growth ledges at such boundaries;
(3) carbide growth increases locally the supersaturation for the sympathetic nucleation of new ferrite crystals and thus the kinetics of such nucleation; and
(4) growth of the sympathetically nucleated crystals occurs until growth ledge density at the same interphase boundary orientation as in (1) again becomes low, thereby encouraging repetition of this cycle.

As Figures 17 and 18 suggest, this sequence does not foreclose continued growth of ferrite around bainitic carbides when the areas of low growth ledge density are sufficiently small so that they can be easily surrounded and overgrown by the adjacent areas of the $\alpha:\gamma$ boundary. However, when a substantial $\alpha:\gamma$ boundary area with a low density of growth ledges reappears, the sympathetic nucleation mechanism will again become operative.

V. SUMMARY

Optical microscopy, quantitative optical metallography, and both replication and transmission electron microscopy have been utilized to investigate the overall reaction kinetics and the morphology of transformation at reaction temperatures between the upper nose (700 °C) in the TTT curve for initiation of transformation and a temperature (525 °C) appreciably below that of the bay (600 °C) in an Fe-0.13 pct C-2.99 pct Cr alloy. Comparison of the transformation kinetics and microstructures with those previously reported in Fe-C-Mo alloys[1,2,5] was one of the principal objectives of this investigation.

At temperatures above that of the bay, T_b, overall transformation kinetics were always of the sigmoidal or Johnson-Mehl[34] type. At all temperatures studied below T_b, three-stage kinetics developed. In the first stage, no carbide precipitation was observed, as in Fe-C-Mo alloys;[2] during the middle stage, transformation ceased entirely, *i.e.*, transformation stasis obtained, and in the third stage, the bainite reaction (not the pearlite reaction) completed decomposition of the austenite matrix. However, instead of stasis appearing at continuously higher percentages of the austenite matrix transformed with increasing undercooling below T_b, as reported in 3 pct Cr steels with various carbon contents by Lyman and Troiano[21] on the basis of dilatometric studies, stasis occurred at 25 pct transformation at 585 °C, 12 pct at 570 °C, 42 pct at 555 °C, and 90 pct at 525 °C. Except for the anomalously high percent transformation at stasis found at 585 °C and the occurrence of the same type of transformation kinetics (Type IV on the scheme of Figure 2(j) and Reference 33) at all temperatures below T_b, the kinetic behavior is similar to that found in Fe-C-Mo alloys.[1,2,5]

Microstructurally, pearlite appeared at 700 °C (the upper nose in the TTT diagram) but not at any lower temperature. A similar lack of interference by the pearlite reaction with transformation phenomena in the vicinity of the bay region obtains in Fe-C-Mo alloys.[1,2,5,16] The Widmanstätten structure diminishes in importance at temperatures below that of the upper nose, as in Fe-C-Mo alloys,[5] but remains present even below T_b. However, a somewhat larger temperature interval obtains below T_b than in Fe-C-Mo alloys before the Widmanstätten structure again becomes pronounced, during which grain and twin boundary allotriomorphs predominate. Again, however, when the Widmanstätten structure resumes its preponderance, it is highly degenerate in seemingly noncrystallographic fashion, also as in Fe-C-Mo alloys.[5] And again, the normal, predominantly plane-sided Widmanstätten structure slowly reappears with further decreases in reaction temperature.

Carbides form in association with the foregoing proeutectoid ferrite structures and also as a component of

nodular bainite. Both interphase boundary and fibrous carbides appear above and below T_b, whereas in an Fe-C-Mo alloy,[13] the fibrous carbides disappear immediately below T_b. Additionally, small amounts of ribbon-shaped carbides and ferrite shoots, associated with carbides, were observed; both have their counterparts in Fe-C-Mo alloys.[45,47] Further evidence was secured with TEM for the formation of the ferritic component of microstructurally defined bainite by sympathetic nucleation at proeutectoid ferrite interfaces rather than by continued growth of ferrite around carbides nucleated at $\alpha:\gamma$ boundaries, as originally proposed by Hultgren.[8] The sympathetic nucleation-based mechanism was previously observed with TEM in a hypoeutectoid Ti-Co alloy.[39]

As in Fe-C-Mo alloys, the SDLE was found to be capable of providing a qualitative explanation for both the reaction kinetics and microstructural phenomena observed. The anomalously high percent transformation at stasis during reaction at 585 °C corresponds directly with the sparsity of the Widmanstätten structure at this temperature and thus with the larger amount of transformation which must occur before the carbon activity in austenite at locations remote from $\alpha:\gamma$ boundaries becomes equal to that at these boundaries. The later carbon activity is appreciably reduced by the SDLE but evidently not sufficiently to halt transformation without the assistance of carbon enrichment of the remaining austenite. The main difference between Fe-C-Mo and Fe-C-Cr alloys in respect to their transformation behavior in the vicinity of T_b is that the SDLE appears to be less effective at a given atomic percent X in the latter alloys. The smaller size difference between Cr and Fe than between Mo and Fe may be responsible for the lesser SDLE in the Fe-C-Cr system.

ACKNOWLEDGMENTS

The contribution of HG was supported by the Conselho Nacional Desenvolvimento Cientifico e Technologico — CNPq-Brazil through Grant No. EM 20-0128/87. Additional support from the USX Corporation and the Air Force Office of Scientific Research through Grant No. AFOSR84-0303 is gratefully acknowledged.

REFERENCES

1. G.J. Shiflet and H.I. Aaronson: *Metall. Trans. A*, 1990, vol. 21A, pp. 1413-32.
2. W.T. Reynolds, Jr., F.Z. Li, C.K. Shui, and H.I. Aaronson: *Metall. Trans. A*, 1990, vol. 21A, pp. 1433-63.
3. F. Wever and H. Lange: *Mitt. Kaiser-Wilhelm-Inst. Eisenforsch.*, 1932, vol. 14, p. 71.
4. R.F. Hehemann, K.R. Kinsman, and H.I. Aaronson: *Metall. Trans.*, 1972, vol. 3, pp. 1077-94.
5. P.G. Boswell, K.R. Kinsman, G.J. Shiflet, and H.I. Aaronson: *Mechanical Properties and Phase Transformations in Engineering Materials*, TMS-AIME, Warrendale, PA, 1986, p. 445.
6. C.A. Dube, H.I. Aaronson, and R.F. Mehl: *Rev. Metall.*, 1958, vol. 55, p. 201.
7. S. Modin: *Jernkontorets Ann.*, 1958, vol. 142, p. 37.
8. A. Hultgren: *Trans. ASM*, 1947, vol. 39, p. 915.
9. W.C. Hagel and M. Ruoff: *Trans. ASM*, 1957, vol. 50, p. 184.
10. H.I. Aaronson and C. Wells: *Trans. AIME*, 1956, vol. 206, p. 1216.
11. ASTM Subcommittee XI: *Proc. Am. Soc. Testing Mater.*, 1950, vol. 50, p. 444.
12. G. Spanos, H.S. Fang, and H.I Aaronson: *Metall. Trans. A*, 1990, vol. 21A, pp. 1381-90.
13. H. Tsubakino and H.I. Aaronson: *Metall. Trans. A*, 1987, vol. 18A, pp. 2047-60.
14. M. Mannerkoski: *Acta Polytech. Scand.*, 1964, ch. 26, p. 7.
15. K. Relander: *Acta Polytech. Scand.*, 1964, ch. 34, p. 7.
16. F.G. Berry and R.W.K. Honeycombe: *Metall. Trans.*, 1970, vol. 1, pp. 3279-86.
17. R.W.K. Honeycombe: *Metall. Trans. A*, 1976, vol. 7A, pp. 915-36.
18. E.S. Davenport and E.C. Bain: *Trans. AIME*, 1930, vol. 90, p.'117.
19. F. Wever and W. Jellinghaus: *Mitt. Kaiser-Wilhelm-Inst. Eisenforsch.*, 1932, vol. 14, p. 105.
20. A. Rose and W. Fischer: *Mitt. Kaiser-Wilhelm-Inst. Eisenforsch.*, 1939, vol. 21, p. 133.
21. T. Lyman and A.R. Troiano: *Trans. ASM*, 1946, vol. 37, p. 402.
22. E.P. Klier and T. Lyman: *Trans. AIME*, 1944, vol. 158, p. 394.
23. K. Campbell and R.W.K. Honeycombe: *Met. Sci.*, 1974, vol. 8, p. 197.
24. H.I. Aaronson: *Trans. TMS-AIME*, 1962, vol. 224, p. 870.
25. H.I. Aaronson and H.A. Domain: *Trans. TMS-AIME*, 1966, vol. 236, p. 781.
26. J.V. Bee, P.R. Howell, and R.W.K. Honeycombe: *Metall. Trans. A*, 1979, vol. 10A, pp. 1207-12.
27. Kehsin Kuo: *J. Iron Steel Inst.*, 1953, vol. 173, p. 363.
28. J.R. Bradley, T. Abe, and H.I. Aaronson: *Rev. Sci. Instrum.*, 1982, vol. 53, p. 98.
29. F.S. Le Pera: *Metallography*, 1979, vol. 12, p. 263.
30. C.K. Shui, W.T. Reynolds, Jr., G.J. Shiflet, and H.I. Aaronson: *Metallography*, 1988, vol. 21, p. 91.
31. T. Gladman and J.H. Woodhead: *J. Iron Steel Inst.*, 1960, vol. 194, p. 189.
32. J.E. Hilliard and J.W. Cahn: *Trans. TMS-AIME*, 1961, vol. 221, p. 344.
33. H.I. Aaronson, W.T. Reynolds, Jr., G.J. Shiflet, and G. Spanos: *Metall. Trans. A*, 1990, vol. 21A, pp. 1343-80.
34. W.A. Johnson and R.F. Mehl: *Trans. AIME*, 1939, vol. 135, p. 416.
35. R.F. Hehemann and A.R. Troiano: *Met. Prog.*, 1956, vol. 70 (2), p. 97.
36. H.I. Aaronson: *Decomposition of Austenite by Diffusional Processes*, Interscience, New York, NY, 1962, p. 387.
37. H.J. Lee, G. Spanos, G.J. Shiflet, and H.I. Aaronson: *Acta Metall.*, 1988, vol. 36, p. 1129.
38. W.T. Reynolds, Jr., H.I. Aaronson, F.Z. Li, and C.K. Shui: *Phase Transformations '87*, Institute of Metals, London, 1988, p. 330.
39. H.J. Lee and H.I. Aaronson: *J. Mater. Sci.*, 1988, vol. 23, p. 150.
40. H.J. Lee and H.I. Aaronson: *Acta Metall.*, 1988, vol. 36, p. 1141.
41. F.G. Berry, A.T. Davenport, and R.W.K. Honeycombe: *The Mechanism of Phase Transformations in Crystalline Solids*, Institute of Metals, London, 1969, p. 288.
42. R.A. Ricks, P.R. Howell, and R.W.K. Honeycombe: *Metall. Trans. A*, 1979, vol. 10A, pp. 1049-58.
43. R.W.K. Honeycombe: *Met. Sci.*, 1982, vol. 14, p. 201.
44. T. Furuhara and H.I. Aaronson: *Scripta Metall.*, 1988, vol. 22, p. 1635.
45. J.V. Bee and D.V. Edmonds: *Metallography*, 1979, vol. 12, p. 3.
46. A. Hultgren: *Kgl. Svenska Vetenskapsakad. Handl.*, 1953, Ser. 4, vol. 4.
47. L.J. Habraken and M. Economopoulos: *Transformation and Hardenability in Steels*, Climax Molybdenum Co., Ann Arbor, MI, 1967, p. 69.
48. E.S.K. Menon and H.I. Aaronson: *Acta Metall.*, 1987, vol. 35, p. 549.
49. K.R. Kinsman and H.I. Aaronson: *Transformation and Hardenability in Steels*, Climax Molybdenum Co., Ann Arbor, MI, 1967, p. 39.
50. H.I. Aaronson, C. Laird, and K.R. Kinsman: *Phase Transformations*, ASM, Metals Park, OH, 1970, p. 313.
51. H.I. Aaronson: *Trans. Indian Inst. Met.*, 1979, vol. 32, p. 1.
52. J.B. Gilmour, G.R. Purdy, and J.S. Kirkaldy: *Metall. Trans.*, 1972, vol. 3, pp. 1455-64.

53. H.I. Aaronson: *The Mechanism of Phase Transformations in Crystalline Solids*, Institute of Metals, London, 1969, p. 270.
54. J.C. Greenbank: *J. Iron Steel Inst.*, 1971, vol. 209, p. 986.
55. J.R. Bradley and H.I. Aaronson: *Metall. Trans. A*, 1981, vol. 12A, pp. 1729-41.
56. H.J. Lee and H.I. Aaronson: *Acta Metall.*, 1988, vol. 36, p. 1155.
57. G. Spanos, H.S. Fang, D.S. Sarma, and H.I. Aaronson: *Metall. Trans. A*, 1990, vol. 21A, pp. 1391-411.
58. N.F. Kennon and N.A. Kaye: *Metall. Trans. A*, 1982, vol. 13A, pp. 975-78.
59. W.T. Reynolds, Jr., S.K. Liu, F.Z. Li, S. Hartfield, and H.I. Aaronson: *Metall. Trans. A*, 1990, vol. 21A, pp. 1479-91.
60. A.T. Davenport and R.W.K. Honeycombe: *Proc. R. Soc.*, 1971, vol. 322, p. 191.
61. V.K. Heikkinnen: *Acta Metall.*, 1973, vol. 21, p. 709.
62. H.I. Aaronson, T. Furuhara, J.M. Rigsbee, W.T. Reynolds, Jr., and J.M. Howe: *Metall. Trans. A*, in press.
63. R.M. Aikin and M.R. Plichta: *Acta Metall.*, 1990, vol. 38, p. 77.
64. H.I. Aaronson and W.T. Reynolds, Jr.: *Phase Transformations '87*, Institute of Metals, London, 1988, p. 301.
65. K.R. Kinsman, E. Eichen, and H.I. Aaronson: *Metall. Trans. A*, 1975, vol. 6A, pp. 303-17.